Torregrosa, AJ.; Galindo, J.; Dolz Ruiz, V.; Royo-Pascual, L. (2016). Dynamic tests and adaptive control of a bottoming organic Rankine cycle of IC engine using swash-plate expander. Energy Conversion and Management. 126:168-176. doi:10.1016/j.enconman.2016.07.078.

DYNAMIC TESTS AND ADAPTIVE CONTROL OF A BOTTOMING ORGANIC RANKINE CYCLE OF IC ENGINE USING SWASH-PLATE EXPANDER

A. Torregrosa, J. Galindo, V. Dolz[1], L. Royo-Pascual

CMT – Motores Térmicos, Universitat Politècnica de València, Spain

R. Haller

Valeo Systèmes Thermiques, La Verrière, France

J. Melis

Exoès, Gradignan, France

Abstract

This paper deals with the experimental testing of a bottoming Organic Rankine Cycle (ORC) integrate in a 2 liter turbocharged gasoline engine using ethanol as working fluid. The main components of the cycle are a boiler, a condenser, a pump and a swash-plate expander. Both steady and transient tests were performed in three engine operating points to understand the behavior and inertia of the system. Pressure-Volume diagram during these transients were presented and analyzed. Operating parameters of the expander, such as expander speed and boiler power, were shifted. The objective of these tests is to understand the inertia of the system and to have a robust control in all the possible transient tests. New European Driving Cycle was tested with and without the expander because

[1] V. Dolz. CMT-Motores Térmicos, Universitat Politècnica de Valencia, Camino de Vera s/n, 46022 Valencia, Spain. Phone: +34 963877650 Fax: +34 963877659 e-mail: vidolrui@mot.upv.es

it is supposed to represent the typical usage of a car in Europe. It was used to validate the control of the ORC in realistic dynamic conditions of the engine. The importance of each parameter was analyzed by fixing all the parameters, changing each time one specific value. The main result of this paper is that using a slightly simple and robust control based on adaptive PIDs, the two dynamic effects of an ORC could be taken into account, i.e. high inertia effects (boiler and condenser) and low inertia effects (pump and volumetric expander).

Keywords

Organic Rankine Cycle, Gasoline engine, Waste Heat Recovery, Swash-plate expander, ethanol, transient tests, NEDC

NOMENCLATURE

Acronyms

BDC	Bottom Dead Centre
CMT	Centro de Motores Térmicos
ICE	Internal Combustion Engine
ORC	Organic Rankine Cycle
PID	Proportional Integral Derivative Controller
PV	Pressure-Volume
SM	Steady-state Map
TEG	Thermoelectric Generator

TDC	Top Dead Centre
WHR	Waste Heat Recovery
NEDC	New European Driving Cycle
FS	Full Scale
WLTC	Worldwide harmonized Light vehicles Test Procedures

Notation

Latin

$\dot{m}$	Mass flow	kg/s
T	Temperature	°C
N	Speed	rpm
P	Power	kW
K_p	Proportional constant	-
K_i	Integral constant	-

Greek letters

$\Delta\dot{m}$	Mass flow increment	kg/s
τ_{exp}	Expander torque	Nm

Subscripts

EG	Exhaust gases side
ET	Ethanol side
W	Water side
in	Inlet conditions
out	Outlet conditions
exp	Expander
$pump$	Pump
$cond$	Condenser
$boil$	Boiler
sat	Saturation conditions
sp	Set point
st	Steady
th	Thermal

1. Introduction

Due to increasingly environmental restrictions and rising fuel prices, higher efficiencies are required to our actual powertrains [1]. Turbocharging technology have CO_2 emissions reduction potential of downsizing engines up to 12% for diesel engines and 14% for gasoline engines [2]. The objective of the turbocharger is to increase torque of the engine and the specific power output with no or slight reductions of bsfc which is less than 1% [3]. Indeed, a turbocharged diesel engine still rejects 35–40% of input energy through the exhaust gas [4]. Therefore, WHR applications can also be found in turbocharged engines. Moreover, new future homologation cycles (such as Worldwide harmonized Light vehicles Test Procedures), will focus on CO_2 emissions, requiring high efficiency increase of the whole drivetrain. In this type of cycles different driving situations on the WLTC are already covered by the hybrid technology: stop and start when the vehicle is stopped (13% of the time) and regenerative breaking system when the vehicle is slowed down (42% of the time). However, the exhaust heat recovery may offer a solution for the remaining time of the cycle (45%) when the engine is loaded [5].

New advanced engine technologies [6], such as electrical and mechanical turbocompounding, thermoelectrical materials (TEG) [7], Heat-to-heat and organic Rankine cycles (ORC) [8], are expected to grow strongly in the coming years [2]. They are considered as a promising source of improvement in modern internal combustion engines (ICE).

Among these technologies, ORC promise high potential [9], therefore, this technology is most widely used in small-scale energy production and industrial applications, i.e. geothermal, biomass, solar thermal power and waste heat recovery (WHR) on industrial processes [10]–[13].

However, the implementation of this technology in modern passenger cars requires additional features to achieve a compact integration and controllability in the engine [14]. While industrial applications typically operates in steady state operating points, there is a huge challenge taking into account its impact in the engine during typical daily driving profiles [15].

Although some experimental papers about ORC in IC engines exist [16]–[19], few experiments have been developed in transient tests. In a previous paper [20], five engine steady-state operating points have been tested using ethanol as working fluid and a swash-plate expander as expander machine. The testing mock up is the same than the one of the articles previously published [21]. The main differences are related to the control of the installation. Before, a state chart was used in order to control the installation by the technician only in stationary conditions. Using these maps of stationary conditions the control was calibrated in order to achieve a robust control in transient operation. The nominal heat input into the boiler in these tested points was 5, 12, 20, 25 and 30 kW respectively. A maximum increase of 3.7% was reached in the ICE mechanical power. In this engine operating point, the expander delivered 1.83 kW. Nowadays the heavy duty industry seem to be clear that they will implement the technology of Rankine Cycle on their long haul trucks before 2020 as an answer to future stringent regulation and the still increasing customers request for operating cost reduction. According to several authors, a 5% fuel economy [22] is achievable when using ethanol as working fluid on such vehicles improving both the expander machine and the evaporator efficiency. This improvement will save approximately 2700 € per year in each truck, avoiding 6 tons of CO_2 emitted to the atmosphere [5].

Despite of these steady experimental studies, experimental transient tests with ethanol in WHR applications have not been published. Some transient models [23]–[26] and experimental installations with water [27] were presented in the literature. However, there is a gap considering ethanol as working fluid and dynamic conditions in an ICE.

Thus, the objective of this paper is to evaluate the transient behavior of an ORC cycle added to an ICE by means of tests realized in our lab using a swash-plate expander and ethanol as working fluid. The partial objectives of this paper are:

- To present the experimental setup.
- To explain in detail the adaptive control of the installation.
- To characterize the transient tests, by changing the inlet conditions of the ORC and understand the behavior of the expander machine during this transients.
- To validate the control of the ORC in realistic dynamic conditions of the engine.

2. Experimental setup

2.1. System layout

Fig 1 shows the schematic diagram of the bottoming ORC cycle. Red lines correspond to the exhaust gas line. The ethanol cycle loop is divided in two colors, green in the high pressure level and black in the low pressure level. Cooling loop is defined by blue lines (dark blue for the inlet cooling line and light blue for the outlet cooling line).

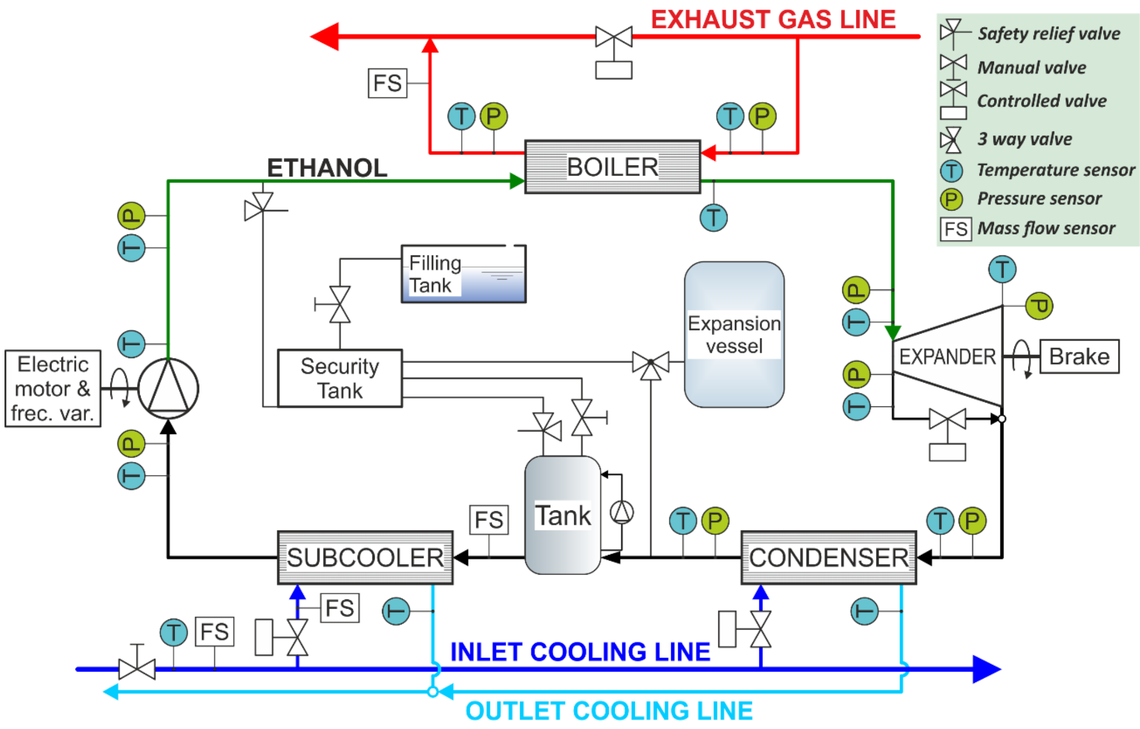

Fig 1. Schematic diagram of the installation

Engine exhaust gases provide heat needed to vaporize the ethanol. Ethanol is a flammable working fluid. Therefore, it is necessary to take the necessary safety measures to prevent accidents arising from the use of this fluid. The gas temperature and mass flow are defined as constant for each particular engine operating point. First, the working fluid is pumped from the tank at the condensing pressure to the boiler at the evaporating pressure. The boiler ensures the heat transfer from exhaust gas to the working fluid. Then, the working fluid is pre-heated, vaporized and superheated in the heat exchanger. The ethanol vapor expands from the evaporating pressure to the condensing pressure. It transforms the enthalpy drop into effective work measured by a torque measuring unit. The expander prototype is a piston swash-plate. Finally, low pressure vapor is extracted from the expander and flows to the condenser, where it condenses using cooling water. The condenser is followed by an expansion vessel in order to insure the low pressure in the installation. It is connected to the circuit by means of a three-way valve to the security tank. In closed loop systems with volumetric machines, it is needed tanks in order to ensure the proper availability of working fluid in all operating points and not to have pressure pulses in the inlet of the expander. The ethanol tank is connected with the security tank. The security tank is used to absorb the working fluid in case the level is increased above the ethanol tank due to pressure pulses. Moreover, this security tank is connected through a manual valve to an additional tank in order to fill the installation.

The geometrical features of the expander are listed in Table 1 and Fig 2 shows a picture of the Swash-plate expander delivered by Exoès.

Table 1. Swash-plate characteristics

Swash-plate characteristics		
Number of pistons	3	
Bore	40	mm
Stroke	31	mm
Maximum expander speed	4500	rpm

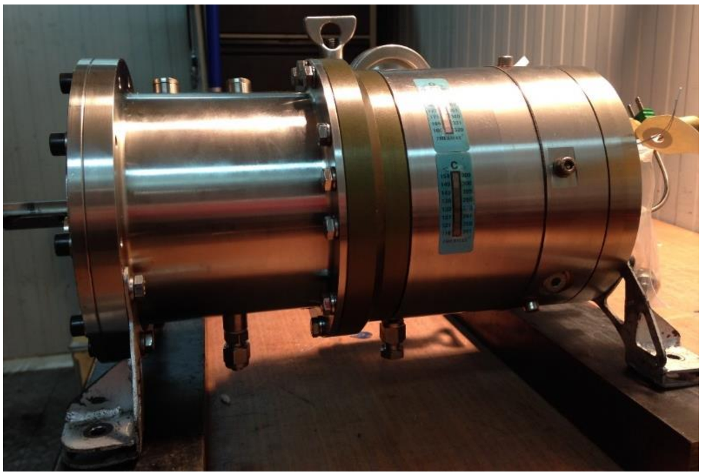

Fig 2. Swash-plate expander delivered by Exoès

Temperature and pressure sensors have been placed at the inlet and the outlet of the different elements, several mass flow sensors have also been installed. Table 2 shows the accuracy, the measurement principle and the range of these sensors.

Table 2. Range and accuracies of sensors

	Measurement principle	Range	Accuracy
Exhaust gas pressure	Piezoresistive	0-2 bar	0.05% FS
Ethanol high pressure loop	Piezoresistive	0-50 bar	0.05% FS
Ethanol low pressure loop	Piezoresistive	0-5 bar	0.05% FS
Temperatures	K-type thermocouples (class 2)	(-270)-(1,372)K	±2.5°C
Ethanol flow meter	Coriolis flow meter	0-2,720 kg/h	±0.1%
Water flow meter	Electromagnetic flow sensor	0.3-1 m/s	±0.5% of rate
Exhaust gases flow meter	Sensyflow FMT700-P	0-500 kg/h	+-1% of rate
Expander rotational speed	Optical tachymeter	0-20,000 rpm	±1 rpm

Expander torque meter	Strain gauges	0-200 Nm	0.05%FS

The expander performance has been characterized by the calculation of the indicated Pressure-Volume diagram. An AVL GU13P piezoelectric pressure sensor was placed inside the cylinder of one piston to evaluate the pressure oscillations during intake and exhaust processes. The piezoelectric transducer was connected to a Kistler 5015 charge amplifier. The PV diagram is used to describe changes of volume and pressure of a system. A swash-plate expander is a positive displacement machine. It works as a two-stroke machine, which means that during one revolution, with a piston movement from the Top Dead Centre to the Bottom Dead Centre and back again, one working cycle is completed. The superheated steam flows through the intake valve into the cylinder whose piston is near top dead centre. Moving the piston downwards, the intake valve closes, the steam expands and let out by exhaust ports situated near the bottom dead centre. Finally, the upmoving piston closes the exhaust ports and compresses the steam remaining in the cylinder and the cycle starts again. Furthermore, a TDC sensor and an angle encoder measure the position of the cylinder. TDC sensor is an eddy current-sensor, which delivers a signal correlating to the distance between sensor and the swashplate. The piezoelectric pressure signal has been referenced using low frequency measurement (piezoresistive sensor). LabVIEW is the software used to record all these signals with a sampling frequency of 50 kHz.

2.2. Operating points

Three engine operating points have been chosen in this tests. The gasoline engine used in these tests is an inline four-cylinder turbocharged engine (Ecoboost) with a volumetric capacity of 2 liter. In a previous article published by the authors [20] five engine operating steady-state points were measured. The vehicle speed was 63 km/h, 84 km/h, 106 km/h, 114 km/h and 126 km/h respectively. These points are representative points of the homologation cycle. However, in the low speed (63 km/h) both the available energy in the exhaust and the potential of recovering is low. Therefore, the viability of this system is achievable at high loads/speeds. Thus, in this article the higher engine operating points (84 km/h, 106 km/h and 114 km/h) were used in order to test the adaptive control. The highest engine operating point was not used in order to avoid possible problems with the control at high ethanol pressure in the system. Fig 3 shows the available exhaust gas energy plotted in the engine map. It was measured at the outlet of the catalyst. This figure also shows the points tested in the ORC. The vehicle model used in the test bench to take into account realistic dynamic conditions of a vehicle was the Ford Explorer. Therefore, these points correspond with 84 km/h (12 kW power in the boiler), 106 km/h (20 kW power in the boiler) and 114 km/h (25 kW power in the boiler). Both steady and transient tests were performed varying from 84 km/h to 114 km/h and from 106 km /h to 114 km/h to understand the behavior and inertia of the system.

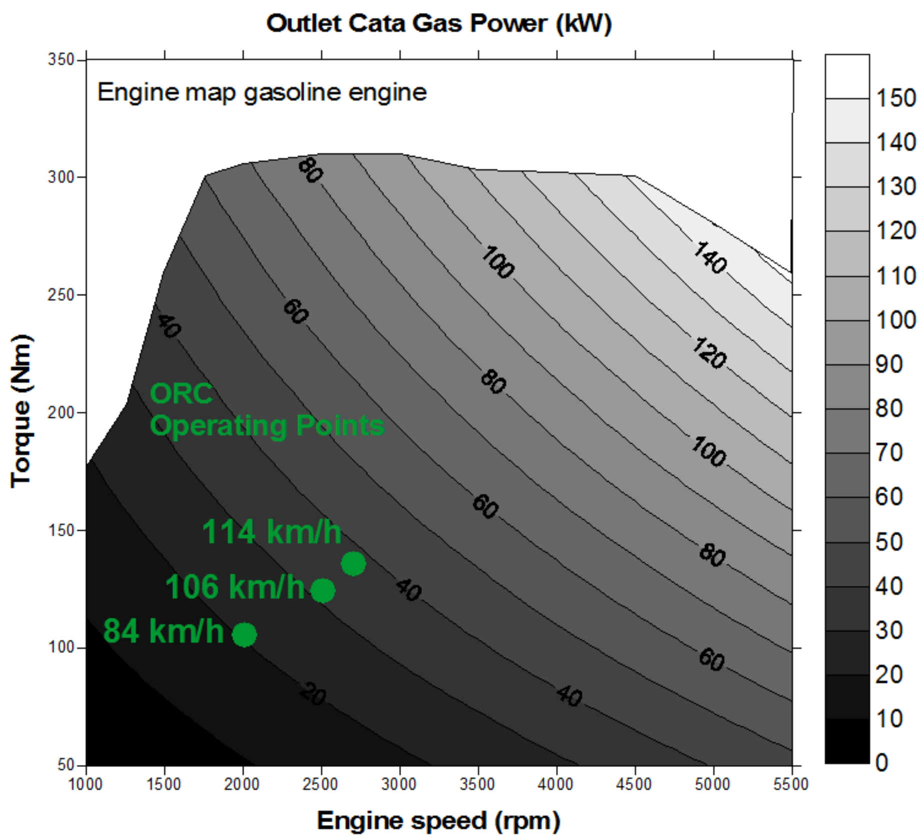

Fig 3. Engine operating points in the ORC

3. Control of the installation

The control of the installation on dynamic conditions has been made using five actuators: IC engine conditions (exhaust gases power), speed of the pump, expander speed, expander vessel pressure (low pressure in the cycle) and the cooling mass flow through the condenser. These actuators can change the behavior of the ORC system:

- Exhaust gases power (P_{EG}), in order to estimate the engine operating point. It was obtained from measuring the exhaust gases temperature at the inlet of the boiler ($T_{In\ Boil\ EG}$) and at the outlet ($T_{Out\ Boil\ EG}$) and the exhaust gases mass flow ($Mflow_{EG}$).

- The speed of the pump (N_{pump}), in order to control the mass flow of ethanol flowing through the installation. It is affected by the exhaust gases power and the temperature at the outlet of the boiler ($T_{ET,out}$).
- The expander speed (N_{exp}), in order to control the high pressure at the inlet of the expander. A brake coupled to the expander shaft fixes this speed. The brake speed is obtained from the exhaust power released in the boiler. Depending on the exhaust gases power, the optimal expander speed was fixed by means of previous parametric studies in steady and optimal conditions for each particular power.
- The expander vessel pressure, in order to control the low pressure in the system.
- The cooling mass flow, in order to avoid cavitation in the pump.

Transient tests were performed changing the exhaust gases power from an initial to a final engine operating point. During the transient, low pressure of the cycle was settled to 2 bar and the cooling mass flow to 672 l/h to avoid cavitation in the pump. The speed of the pump (N_{pump}) and the speed of the expander (N_{exp}) have been controlled by using an adaptive control, presenting in Fig 4. Red arrows correspond to inputs of the system, while blue ones correspond to outputs. Different steady-state maps, obtained from previous steady tests [20], were implemented in the control. Table 3 summarizes the inputs and outputs of the system.

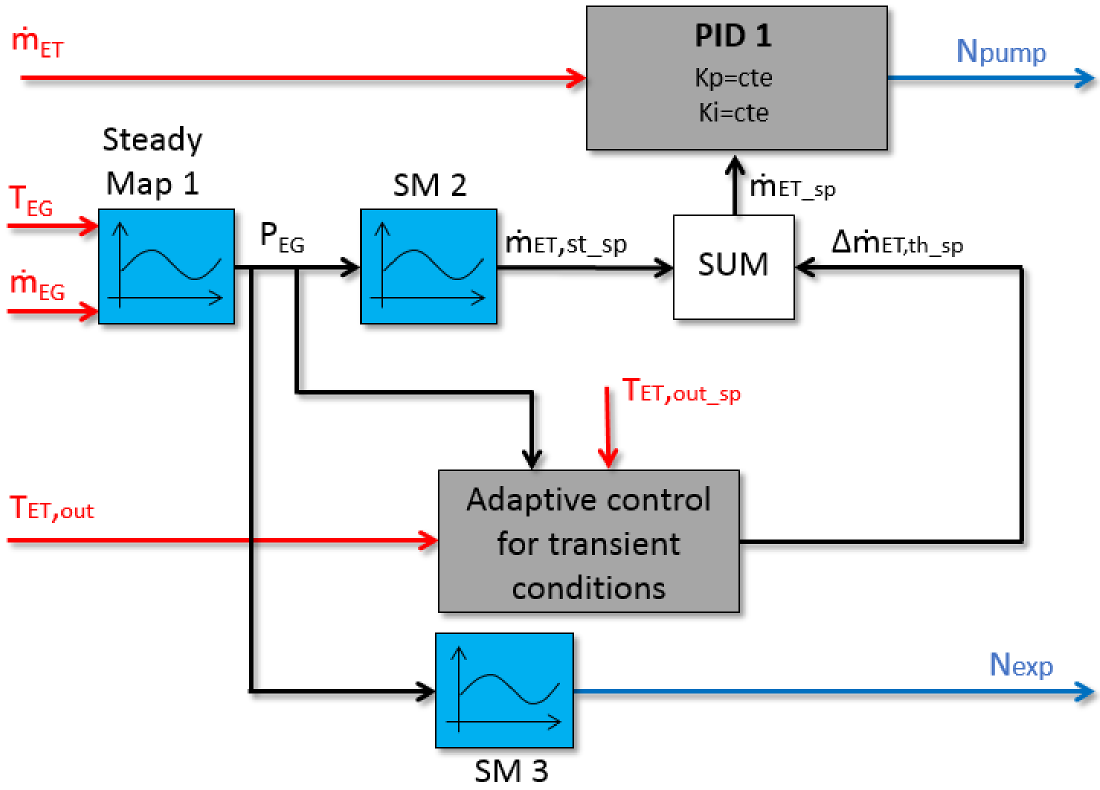

Fig 4. Control of the installation

Table 3. Inputs and outputs of the ORC control

Variable name	Description	I/O
$\dot{m}_{ET}$	Ethanol mass flow	Input
T_{EG}	Exhaust gases temperature (inlet and outlet)	Input
$\dot{m}_{EG}$	Exhaust gases mass flow	Input
$T_{ET,out}$	Temperature at the outlet of the boiler	Input
T_{ET,out_sp}	Temperature at the outlet of the boiler set point	Input
N_{pump}	Pump speed	Output
N_{exp}	Expander speed	Output

The mass flow ($\dot{m}_{EG}$) and the temperatures at the inlet and outlet of the boiler (T_{EG}) in the exhaust gases side were measured; therefore, an estimation of the power released by the exhaust gases was obtained (P_{EG}) by using steady-state map (SM 1). In the ethanol side, both the ethanol mass flow ($\dot{m}_{ET}$) and the temperature at the outlet of the boiler ($T_{ET,out}$) were inputs of the control.

Using steady-state map (SM 2), an initial ethanol mass flow set point was specified ($\dot{m}_{ET,st\_sp}$). However, in the steady tests, as the thermodynamic variables vary smoothly, the control system does not take into account effects of transients. During transient conditions, once the operating point is changed, the control should consider two interconnected phenomena: Low inertia elements (pump and volumetric expander) and high inertia elements (boiler and condenser). Therefore, in an ORC system, changes in the pump and expander speed have a fast time response (lower than 1 s), because they affect mainly to pressures and mass flows in the system. However, changes in the heat transferred by the heat exchangers (boiler and evaporator) have a higher time response (40 s) because its main function is to heat or cool down the ethanol, and therefore they affect mainly to the temperatures in the system. Thus, an adaptive part of the control corrects the ethanol mass flow set point of steady conditions to take into account the high inertia elements. The correction ($\Delta\dot{m}_{ET,th\_sp}$) was applied to the initial ethanol mass flow ($\dot{m}_{ET,st\_sp}$). The result signal ($\dot{m}_{ET,sp}$) is compared to the actual ethanol mass flow through the system (measured by a Coriolis mass flow meter) and using PID 1 the pump speed set point for transient conditions is obtained (N_{pump}).

The correction ($\Delta\dot{m}_{ET,th\_sp}$) takes into account the dynamic conditions of the boiler and deviation between the temperature signal at the outlet of the boiler ($T_{ET,out}$) and the ethanol temperature reference of steady conditions, setting by an external threshold T_{ET,out_sp}. This temperature is fixed by the working fluid in order to avoid degradation. In these tests, the working fluid was ethanol; therefore, the maximum temperature was 240 ºC. However, in these particular tests the temperature was 210 ºC in order to ensure a stable operation of the working fluid.

The adaptive control consists of two inputs (P_{EG} and ΔT) and two outputs corresponding to the proportional and integral constant of the PID (K_p and K_i). Depending on the exhaust power required and the difference of temperatures between the measurement ($T_{ET,out}$) and the set point (T_{ET,out_sp}) a specific value for Kp and Ki was obtained. Values of adaptive control were progressively adjusted from experimental tests. Different values of Kp and Ki were implemented in the control to avoid condensation at the expander inlet when the engine operating point changes from a lower to a higher exhaust power and superheating (and thus degradation) in the opposite case. When the engine operating point changes from a lower to a high power, the ethanol mass flow should not change rapidly because the boiler is not hot enough and condensation could appear if there is not enough power to maintain the temperature at the outlet of the boiler. Regarding the expander, a steady state map (SM 3) was used to fix the optimum expander speed for each boiler power (P_{EG}).

4. Transient tests PV diagram

Two transient tests were performed in the cycle measuring the instantaneous pressure inside the cylinder of the swash-plate, varying the vehicle speed from 84 km/h (12 kW power in the boiler) to 114 km/h (25 kW in the boiler) and from 106 km/h (20 kW) to 114 km/h (25 kW). The time step between the two engine operating points was set to 5 s in order to test the most severe conditions to the engine and to the ORC.

4.1. Transient 12-25 kW with 5 s

The main actuators of the system are presented in Fig 5. The first subplot (A) indicates the pressure in the expansion vessel ($P_{Ex\ Cond}$). The second subplot (B) indicates the temperatures in the exhaust line, inlet temperature of the boiler ($T_{In\ Boil\ EG}$) in the left axis and outlet temperature of the boiler ($T_{Out\ Boil\ EG}$) in the right axis. The third subplot (C) indicates the mass flow through the system, the exhaust gases mass flow ($Mflow_{EG}$) in the left axis and the cooling mass flow (Mflow W) in the right axis. The last subplot (D) indicates the pump speed (N_{pump}) in the left axis and the expander speed (N_{exp}) in the right axis. In this transient test, the vehicle speed was shifted from 84 km/h to 114 km/h. As it can be seen in Fig 5, the exhaust gas mass flow increases from 100 kg/h to approximately 150 kg/h. The exhaust gas step starts approximately in second 15. The water mass flow remains constant with a value of 690 kg/h. Both expander and pump speed changes according the control previously presented. The colored vertical lines correspond to particular times of the transient tests that will be deeply analyzed on next paragraphs of this paper.

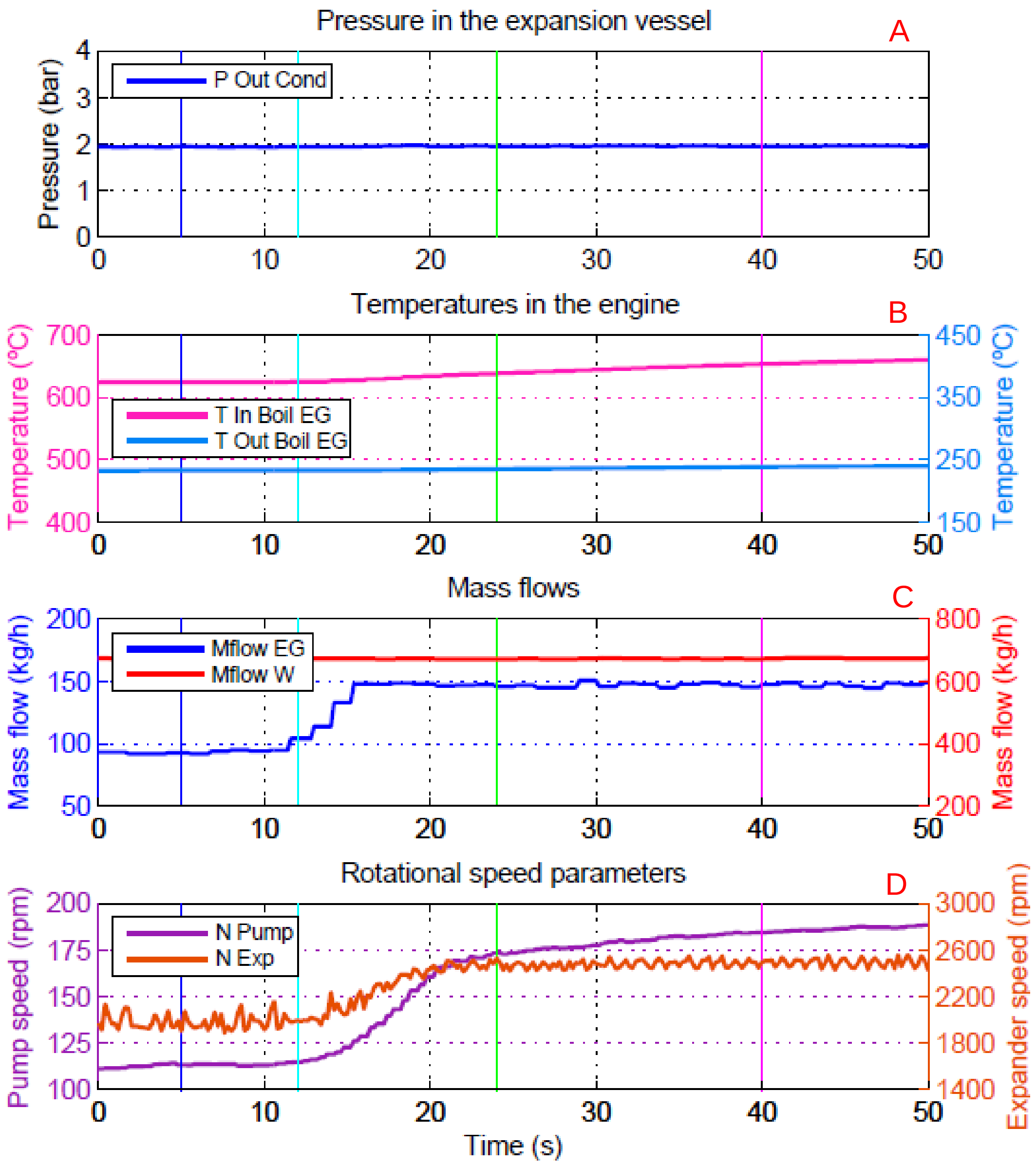

Fig 5. Actuators of the ORC transient 12-25 kW (5s)

The main output variables of the cycle are presented in Fig 6. The first subplot (A) indicates pressures in the ORC, HP ($P_{In\ Exp\ ET}$) in the left axis and LP ($P_{Ex\ Exp\ ET}$) in the right axis. The second subplot (B) indicates the temperature at the inlet of the swash-plate expander ($T_{In\ Exp\ ET}$), the saturation temperature (T_{sat}) and the temperature at the outlet of the expander ($T_{Ex\ Exp\ ET}$). The third subplot (C) indicates the ethanol mass flow through the system ($Mflow_{ET}$). The last subplot (D) indicates the torque (τ_{exp}) and the expander speed (N_{exp}). As explained in the control of the installation, the expander speed was optimized for each particular exhaust gas power; therefore, while the engine operating point was shifted from 12 kW to 25 kW the expander speed was varied from 2000 rpm to 2500 rpm. As higher power is released in the exhaust gases, the ethanol is vaporized into a higher level of pressure. Temperature at the boiler outlet remains almost constant due to the reference threshold of the control that fix 210 ºC as a set point. Ethanol mass flow increased considering both dynamic effects: high and low inertia elements. Torque delivered by the expander increases with exhaust gases power, as the nominal ethanol mass flow through the system increases. The isentropic efficiency remains constant because although the power delivered by the expander increases, the expansion ratio increases too, therefore the relation between isentropic and shaft power remains almost constant. The expander speed is also changing from 2000 rpm to 2500 rpm.

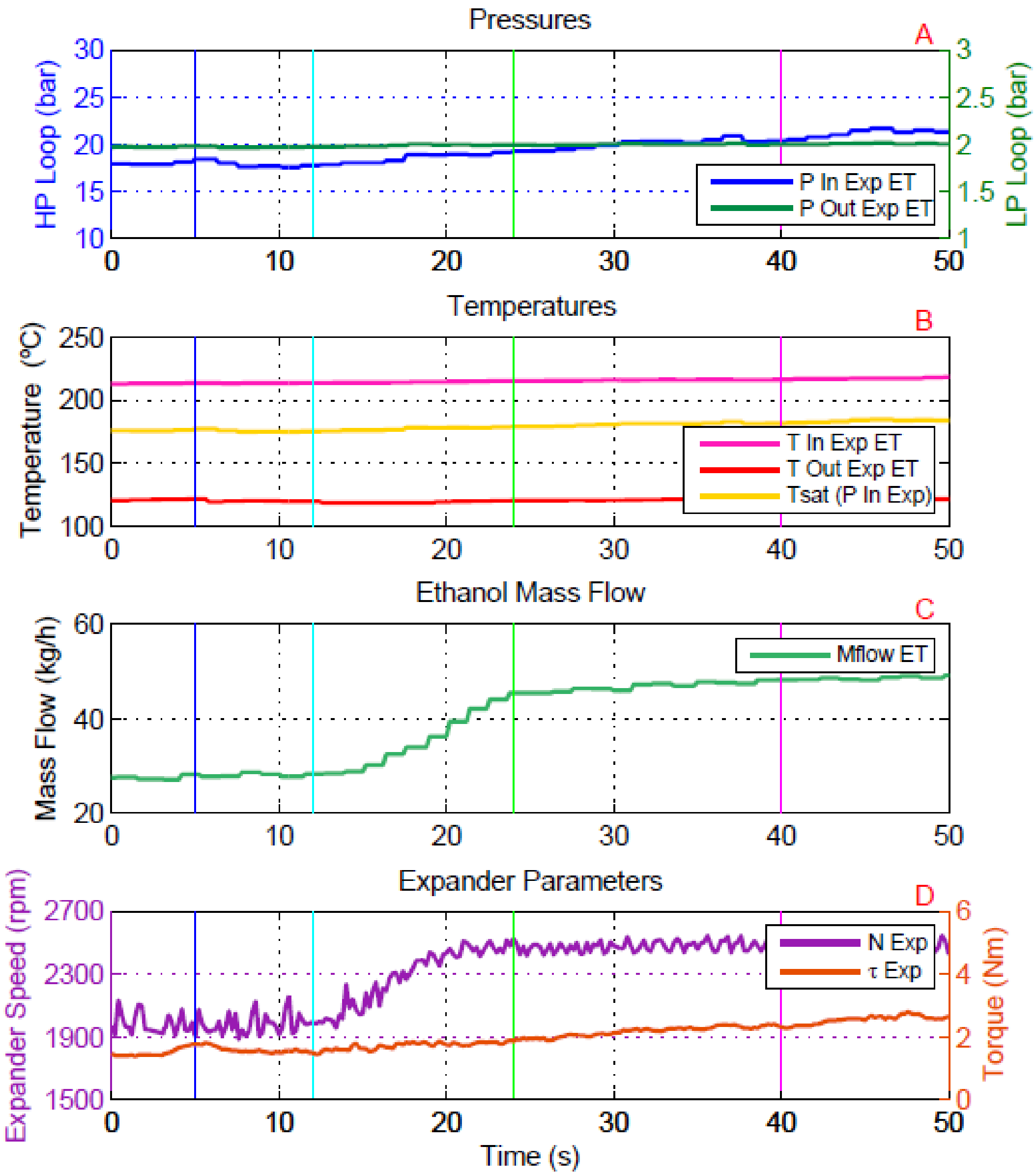

Fig 6. Main parameters in the ORC transient 12-25 kW (5s)

The analysis of PV diagrams in different conditions during the transient could be convenient to evaluate possible irreversibilities in the expansion machine. The PV diagram has been computed in 4 specific instants of time during the transient. The instances were chosen to represent initial steady-state, start of transient, end of transient and final steady-state (5 s, 12 s, 24 s and 40 s):

- t=5 s: Initial steady state point at the lower engine operating point (12 kW). All the variables of the system remain constant and the expander speed is 2000 rpm.
- t=12 s: Start of the transient test. The ethanol mass flow is increasing to adapt the ORC to the new engine operating point (25 kW). Pressures are increasing and expander speed is changing from 2000 rpm to 2500 rpm.
- t=24 s: End of the transient test. The ethanol mass flow has almost reached the new operating conditions. Pressure continues increasing. Expander speed is 2500 rpm.
- t=40 s: Steady state at the new operating conditions of the engine (25 kW). All the variables of the system remain almost constant and the expander speed is 2500 rpm.

These points have been indicated in Fig 5 and Fig 6 using vertical lines with the same colors that the PV plots of Fig 7. In order to estimate the PV diagram of a specific time of the transient, an average of a finite number of cycles have been computed. On one hand, a low number of cycles won't be representative because of the deviation in measurements. On the other hand, if a high number of cycles is taken into account, the PV diagram area will increase as a consequence of the change in the engine operating point. Therefore, a sensitivity study was done to determine the optimal number of cycles to average the area in the PV diagram during these cycles. As a result of this parametric study, the average indicated power remains constant in the range from 80 to 110 cycles. Thus, 80 cycles were chosen to reduce the CPU calculation time. This parametric study was made in the middle of the transient (t=18 s) to consider a high level of variability.

Fig 7 shows the PV diagram in the previous time instances. Red and green crosses indicate the intake and exhaust valve closing angles (or volumes) respectively. Red and green circles indicate the intake and exhaust valve opening angles (or volumes) respectively. By comparing all the diagrams, it can be seen that the compression process in the piston (PV slope during compression process) is more isothermal at lower expander speeds (at time 5 s, 2000 rpm) than at higher expander speeds (at time 12 s, 24 s and 40 s, 2500 rpm). Lower expander speeds involve higher heat transfer rates, therefore more isothermal compression process.

Focusing on the maximum pressure reached by the system (at time 12 s, 24 s and 40 s) it can be seen that higher exhaust power has a direct impact on the maximum pressure of the PV diagram. This effect justifies the increase on the high pressure of the cycle and the thermal behavior of the system. Once the engine operating point is shifted, the thermal delay of the boiler causes that although the mass flow transient is finished, the indicated diagram continues increasing to higher levels of pressure. This effect is visible comparing 24 s and 40 s indicated diagrams.

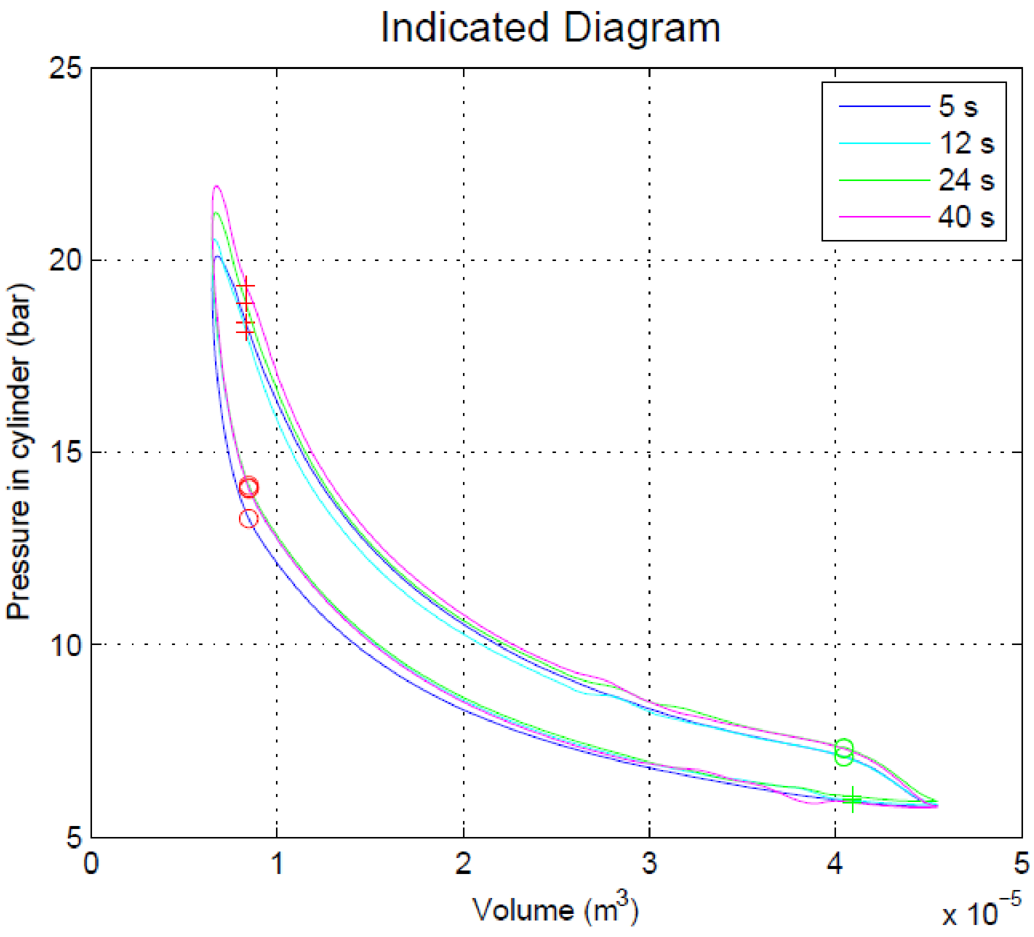

Fig 7. P-V Diagram transient tests 12-25 kW (5s)

4.2. Transient 20-25 kW with 5 s

Fig 8 and Fig 9 show respectively the actuators and the main parameters of the cycle for the transient 20-25 kW. The main actuators of the system are presented in Fig 8. The first subplot (A) indicates the pressure in the expansion vessel ($P_{Ex\ Cond}$). The second subplot (B) indicates the temperatures in the exhaust line, inlet temperature of the boiler ($T_{In\ Boil\ EG}$) in the left axis and outlet temperature of the boiler ($T_{Out\ Boil\ EG}$) in the right axis. The third subplot (C) indicates the mass flow through the system, the exhaust gases mass flow ($Mflow_{EG}$) in the left axis and the cooling mass flow (Mflow W) in the right axis. The last subplot (D) indicates the pump speed (N_{pump}) in the left axis and the expander speed (N_{exp}) in the right axis. In this transient test, the vehicle speed was shifted from 106 km/h to 114 km/h. As it can be seen in Fig 8, the exhaust gas mass flow increases from 120 kg/h to approximately 150 kg/h. The exhaust gas step starts approximately in second 15. The water mass flow remains constant with a value of 690 kg/h. In this case, the expander speed is constant (2500 rpm).

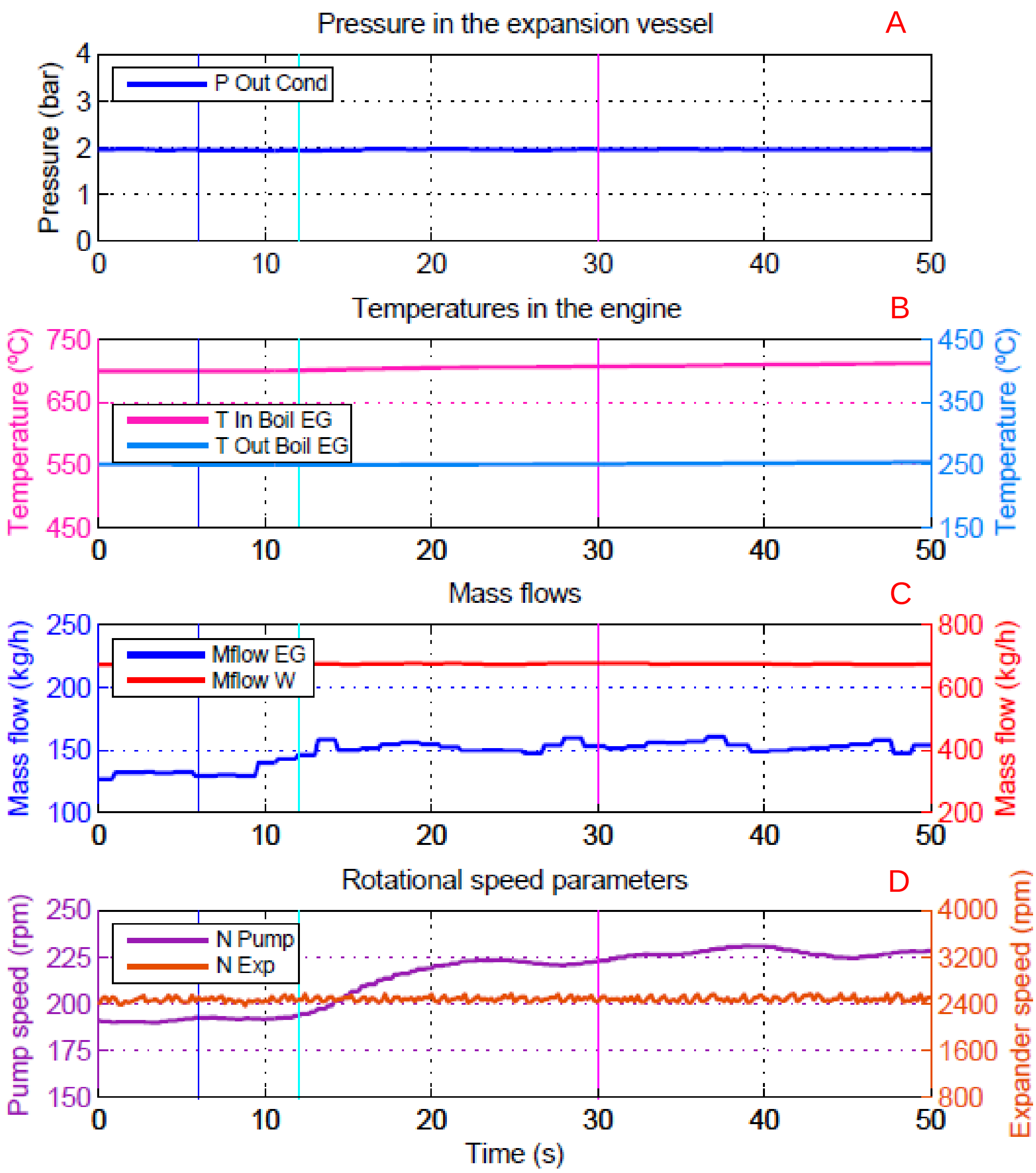

Fig 8. Actuators of the ORC transient 20-25 kW (5s)

The main output variables of the cycle are presented in Fig 9. The first subplot (A) indicates pressures in the ORC, HP ($P_{In\ Exp\ ET}$) in the left axis and LP ($P_{Ex\ Exp\ ET}$) in the right axis. The second subplot (B) indicates the temperature at the inlet of the swash-plate expander ($T_{In\ Exp\ ET}$), the saturation temperature (T_{sat}) and the temperature at the outlet of the expander ($T_{Ex\ Exp\ ET}$). The third subplot (C) indicates the ethanol mass flow through the system ($Mflow_{ET}$). The last subplot (D) indicates the torque (τ_{exp}) and the expander speed (N_{exp}).

The expander was optimized at 2500 rpm in both exhaust gas power. As higher power is released in the exhaust gases, the ethanol is vaporized into a slightly higher level of pressure. Changes are lower than in the previous transient due to lower differences in the transient. Temperature at the boiler outlet remains at the same level of 210 ºC. Ethanol mass flow increased considering both dynamic effects: high and low inertia elements. Torque delivered by the expander increases with exhaust gases power, as the nominal ethanol mass flow through the system increases.

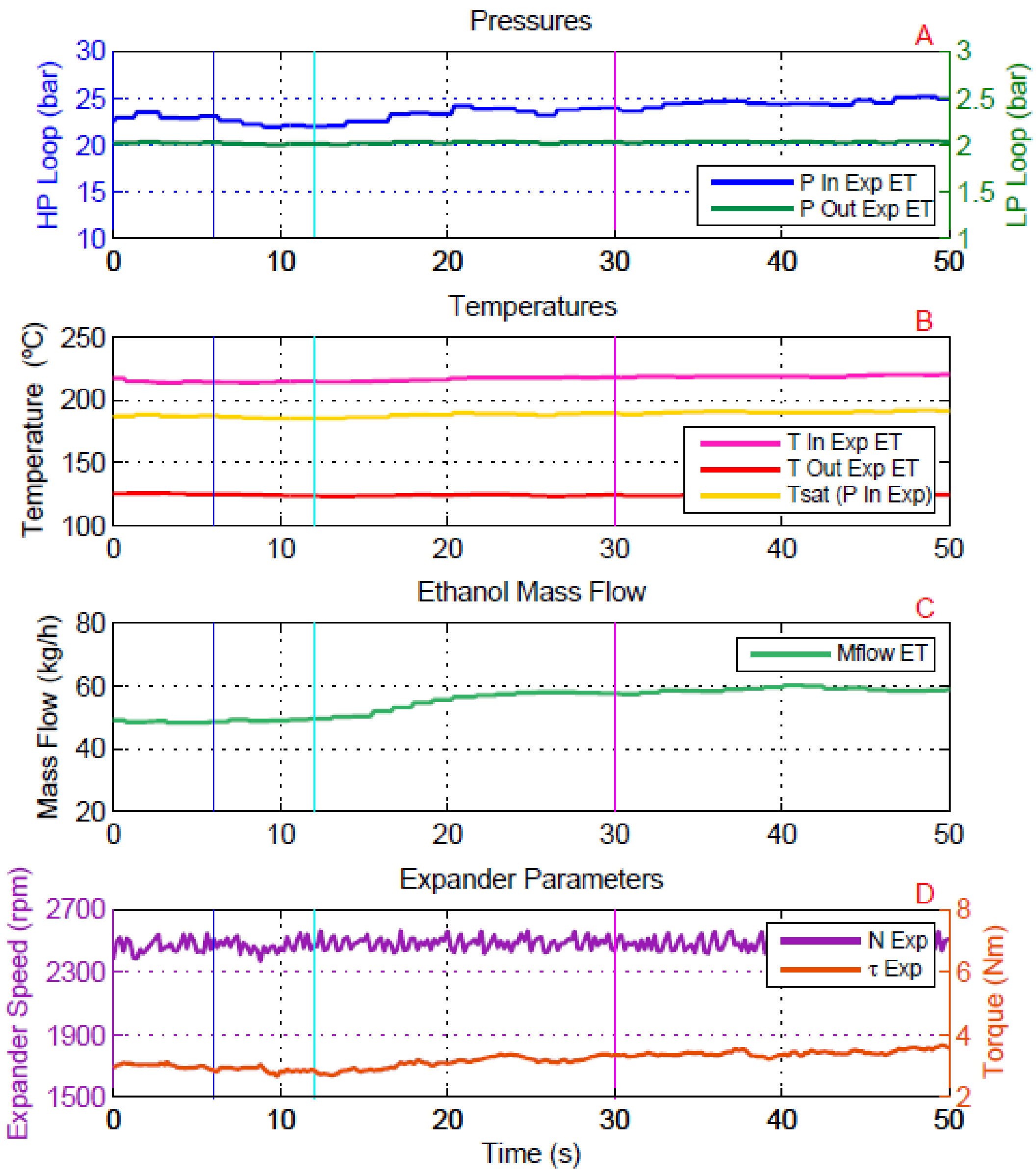

Fig 9. Main parameters in the ORC transient 20-25 kW (5s).

The PV diagram has been computed in 3 specific instants of time during the transient. The instances were chosen to represent initial steady-state, start of transient and the end of transient (6 s, 12 s and 30 s):

- t=6 s: Initial steady state point at the lower engine operating point (20 kW). All the variables of the system remain constant and the expander speed is 2500 rpm.

- t=12 s: Start of the transient test. The ethanol mass flow is increasing to adapt the ORC to the new engine operating point (25 kW). Pressures are increasing while the expander speed remains constant.
- t=30 s: End of the transient test. The ethanol mass flow has almost reached the new operating conditions. Pressure continues increasing. Expander speed is 2500 rpm.

Fig 10 shows the PV diagram at different instants of time during the test. By comparing all the diagrams, it can be observed that the compression process in the piston remains more or less similar (in second 6 s, 12 s and 30 s) due to the expander speed remains constant during this test.

As regards the maximum pressure reached by the system, it can be seen that higher exhaust power has a direct impact on the maximum pressure of the PV diagram. Therefore, the more power it is released on the boiler, the higher amount of indicated power it is produced. The expansion laws are approximately equal; however, the inlet valve closes at higher level of pressure when time increases, therefore, the area of the PV diagram increases with time.

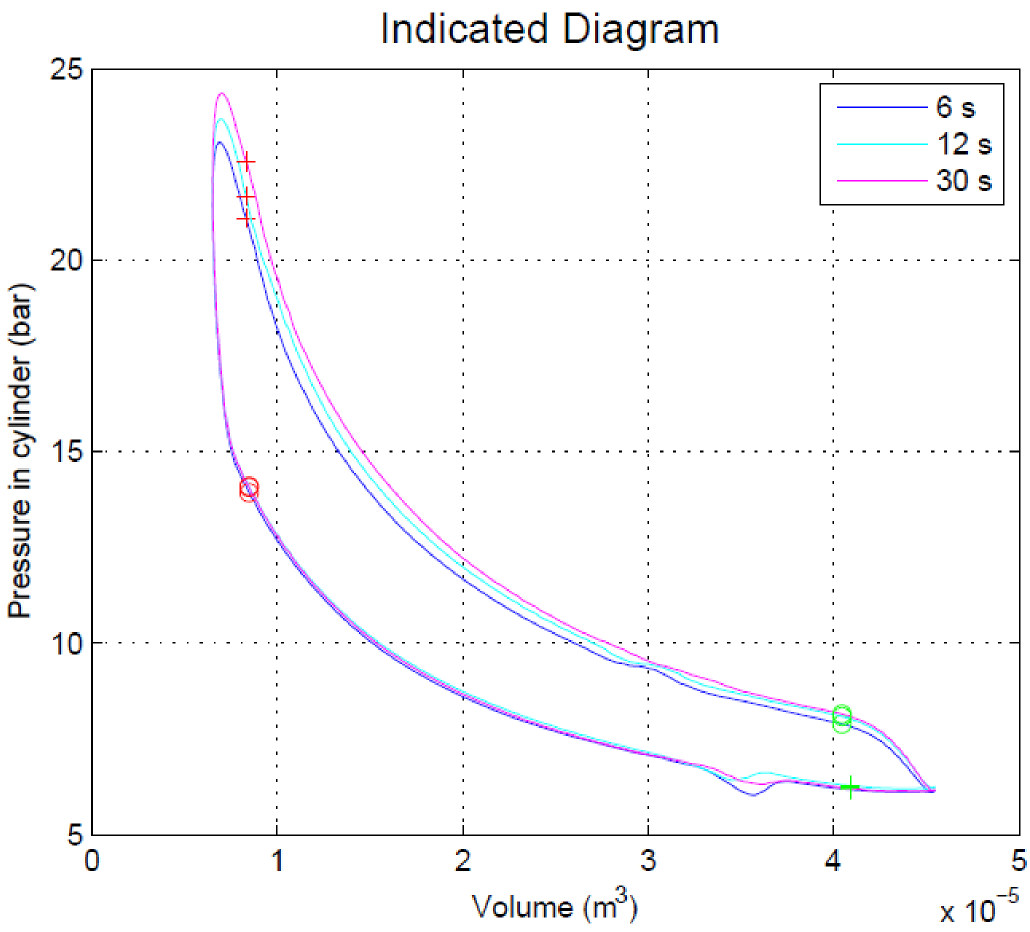

Fig 10. P-V Diagram transient tests 20-25 kW (5s)

To sum up, taking into account previous analysis, the control of the system should consider both phenomena, high inertia effects (boiler and condenser) and low inertia effects (pump and volumetric expander). A delay is visible analyzing the PV diagram of the expander machine. The temperature at the outlet of the boiler is fixed to 210 ºC, therefore the boiler delay is visible in the pressure signal. As a result, although the conditions of mass flow changes promptly, the thermal inertia of the system cause the cycle a delay in pressures. The final control of the ORC should consider these effects. Therefore, the adaptive correction introduced in the control of the cycle is justified with previous analysis, as shown in Fig 4.

A statistical analysis of the work delivered by the expander in J during the transient 20-25 kW is presented in Table 4. In this table the average work delivered by the expander, the standard deviation, the maximum and the minimum values are shown in the same time analyzed previously (6 s, 12 s and 24 s). The average work delivered by the expander increases from 11.101 J to 12.832 J as a result of the change in the engine operating point. Regarding the standard deviation, it remains approximately constant with a maximum value of 0.781 J in the second 12. Similar results were obtained with the transient 12-25 kW.

Table 4. Statistical analysis transient 20-25 kW

Time	Work delivered by the expander (J)	Standard Deviation (J)	Max	Min
6 s	11.101	0.711	12.708	9.829
12 s	12.309	0.781	14.074	9.829
24 s	12.832	0.552	13.873	11.718

5. NEDC cycle

5.1. Available energy in the NEDC

In order to apply the control of the installation to realistic driving conditions, the engine was tested following the New European Driving Cycle (NEDC). The purpose of this test was to estimate the amount of power released by the exhaust gases during this cycle and estimate the points in which the expander could be started. Fig 11 shows the result of this test. During the urban part of the cycle, there is not enough power in the cycle to evaporate and produce power in the expander, because the engine is in warm up conditions and temperatures are too low. The vapor conditions at the boiler outlet begins approximately at second 900. Although the exhaust gas mass flow changes very fast, the response in temperature in the exhaust line is slower. The time response in temperatures is approximately 40 s, whereas in mass flows is in the range of 5 s, as it can be seen in Fig 5 and Fig 8 . Moreover, the installation response to the NEDC is well controlled with the control layout performed.

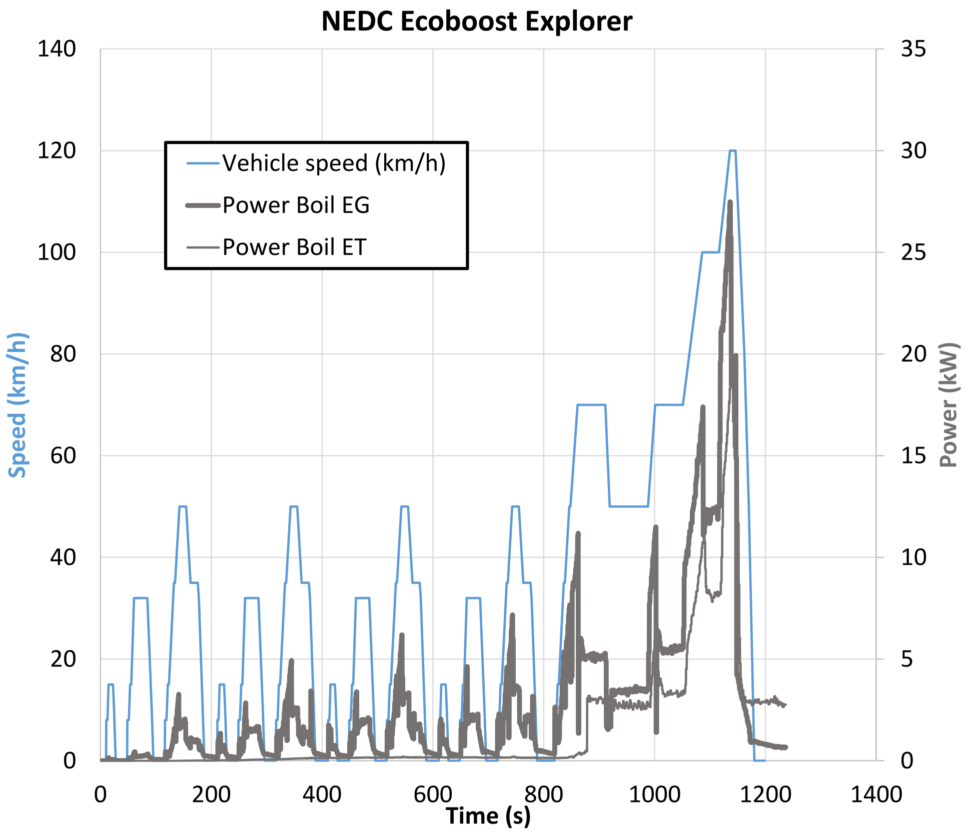

Fig 11. NEDC without expander

As the urban cycle starts from idle and cold conditions and reaches the high power in few minutes, there is no enough time to deliver enough power to the expander. Therefore, it can be concluded that NEDC cycle is not the optimal cycle to test this type of technology. High loads and hot conditions should be the starting ideal conditions to test and validate the control of the ORC proposed in this paper.

5.2. Validation of the control in optimal driving profile

Considering the results obtained in previous section, the last part of the NEDC, starting at hot conditions, was tested. It corresponds to extra-urban cycle (the last acceleration from 70 km/h to 120 km/h of NEDC) after stabilizing during some minutes the point of 70 km/h. Fig 12 shows the result of this test with the expander. In this case, there is enough power in the cycle to evaporate the ethanol and start the expander.

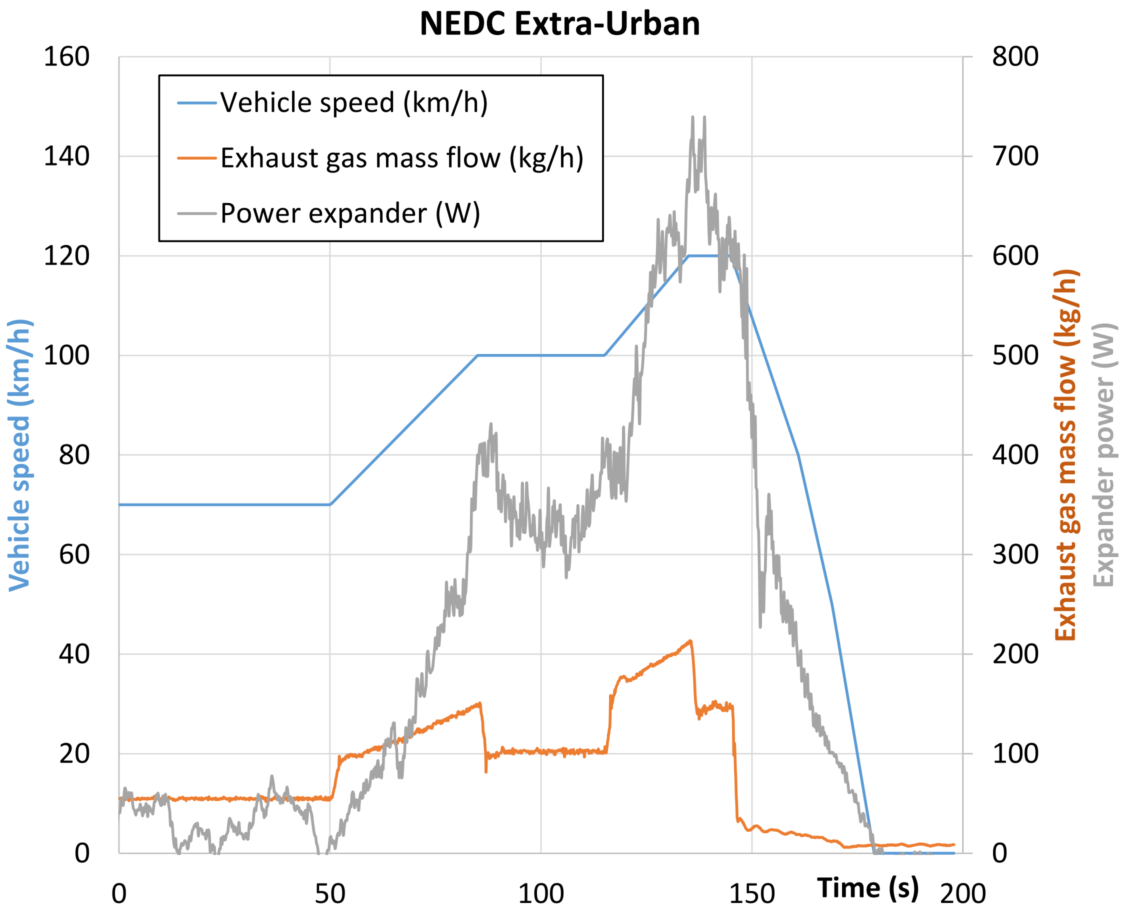

Fig 12. NEDC Extra-Urban with expander

The main conclusion of this test is that using a slightly simple and robust control based on adaptive PIDs, the two dynamic effects of an ORC could be taken into account, i.e. high inertia effects (boiler and condenser) and low inertia effects (pump and volumetric expander). Therefore, the control of the ORC was validated in realistic dynamic conditions of the engine.

6. Conclusions

This paper describes and analyzes the results of an experimental installation of an ORC system installed in a turbocharged 2.0 liter gasoline engine to recover waste heat in exhaust gases. Both, steady tests in three engine operating points, and transient tests varying from 84 km/h (12 kW) to 114 km/h (25 kW) and from 106 km /h (20 kW) to 114 km/h (25 kW) were performed in order to understand the behavior and inertia of the system. The PV diagram during these transients were presented and analyzed. The following results have been obtained with available components based on non-commercial prototypes:

1. The installation response to dynamic transient tests (12-25 kW and 20-25 kW) is well controlled with the control layout performed with engine time steps up to 5s. NEDC extra urban transient cycle was performed using the same control obtaining a controllable system.
2. The control of the system considers both high inertia effects (boiler and condenser) and low inertia effects of volumetric machines. The adaptive control lets the system adapt to these dynamic operating conditions of the engine.
3. Compression in the piston is more isothermal at lower expander speeds than at higher expander speeds. Lower expander speeds involve higher residence time of ethanol inside the cylinders. Consequently, heat transfer rates increases with lower expander speeds. Therefore, lower expander speeds involve more isothermal compression process. The more power is released by the boiler, the higher amount of indicated power is produced by means of higher pressure at the inlet of the expander machine.

4. NEDC cycle produce not enough power to run the expander in normal operating conditions starting from engine cold conditions. High loads and hot conditions should be the starting ideal conditions to test and validate the control of the ORC.
5. The slightly simple and robust control presented in this paper, based on adaptive PIDs, allows the control of the ORC in realistic driving profiles.

7. Acknowledgements

This work is part of a research project called “Evaluation of bottoming cycles in IC engines to recover waste heat energies” funded by a National Project of the Spanish Government with reference TRA2013-46408-R. The authors thank also to Raul Lujan and Rafael Carrascosa for their contribution in the testing process. Authors want to acknowledge the “Apoyo para la investigación y Desarrollo (PAID)” grant for doctoral studies (FPI S2 2015 1067).

REFERENCES

[1] F. Payri, J. Luján, C. Guardiola, and B. Pla, “A Challenging Future for the IC Engine: New Technologies and the Control Role,” *Oil Gas Sci. Technol. – Rev. d’IFP Energies Nouv.*, vol. 70, no. 1, pp. 15–30, Jun. 2014.

[2] R. Berger, “Trends in ICE-Technologies Besides Electrification , improvements in conventional powertrain technologies will play a major role looking forward,” in *Automotive megatrends*, 2013, pp. 1–13.

[3] J. B. Heywood, *Internal combustion engine fundamentals*. 1988.

[4] S. N. Hossain and S. Bari, “Waste heat recovery from the exhaust of a diesel generator using Rankine Cycle,” *Energy Convers. Manag.*, vol. 75, pp. 141–151, 2013.

[5] R. Daccord, A. Darmedru, and J. Melis, “Oil-Free Axial Piston Expander for Waste Heat Recovery,” *SAE Int.*, vol. 14HX, pp. 1–12, Apr. 2014.

[6] R. Saidur, M. Rezaei, W. K. Muzammil, M. H. Hassan, S. Paria, and M. Hasanuzzaman, “Technologies to recover exhaust heat from internal combustion engines,” *Renew. Sustain. Energy Rev.*, vol. 16, no. 8, pp. 5649–5659, Oct. 2012.

[7] S. Riffat and X. Ma, “Thermoelectrics: a review of present and potential applications,” *Appl. Therm. Eng.*, vol. 23, no. 8, pp. 913–935, Jun. 2003.

[8] T. Al-Shemmeri, *Engineering Thermodynamics*, vol. 181, no. 4615. 2010.

[9] M. Bianchi and A. De Pascale, “Bottoming cycles for electric energy generation: Parametric investigation of available and innovative solutions for the exploitation of low and medium temperature heat sources,” *Appl. Energy*, vol. 88, no. 5, pp. 1500–1509, May 2011.

[10] V. Zare, “A comparative exergoeconomic analysis of different ORC configurations for binary geothermal power plants,” *Energy Convers. Manag.*, vol. 105, pp. 127–138, Nov. 2015.

[11] A. Borsukiewicz-Gozdur, S. Wiśniewski, S. Mocarski, and M. Bańkowski, “ORC power plant for electricity production from forest and agriculture biomass,” *Energy Convers. Manag.*, vol. 87, pp. 1180–1185, Nov. 2014.

[12] A. M. Delgado-Torres and L. García-Rodríguez, “Analysis and optimization of the low-temperature solar organic Rankine cycle (ORC),” *Energy Convers. Manag.*, vol. 51, no. 12, pp. 2846–2856, Dec. 2010.

[13] F. Campana, M. Bianchi, L. Branchini, A. De Pascale, A. Peretto, M. Baresi, A. Fermi, N. Rossetti, and R. Vescovo, “ORC waste heat recovery in European energy intensive industries: Energy and GHG savings,” *Energy Convers. Manag.*, vol. 76, pp. 244–252, Dec. 2013.

[14] A. Hernandez, A. Desideri, C. Ionescu, and S. Quoilin, “Towards the optimal operation of an Organic Rankine Cycle unit by means of model predictive control,” *3rd Int. Semin. ORC Power Syst.*, pp. 1–10, 2015.

[15] M. C. Robertson, A. W. Costall, P. J. Newton, and R. F. Martinez-botas, “Transient duty cycle analysis for mobile Organic Rankine Cycle applications,” *3rd Int. Semin. ORC Power Syst.*, pp. 1–10, 2015.

[16] T. Park, H. Teng, G. L. Hunter, B. van der Velde, and J. Klaver, “A Rankine Cycle System for Recovering Waste Heat from HD Diesel Engines - Experimental Results,” *SAE Int.*, vol. 1, pp. 1–9, Apr. 2011.

[17] T. Endo, S. Kawajiri, Y. Kojima, K. Takahashi, T. Baba, S. Ibaraki, T. Takahashi, and M. Shinohara, “Study on Maximizing Exergy in Automotive Engines,” *SAE Int.*, vol. 1, pp. 1–12, 2007.

[18] H. Teng, G. Regner, and C. Cowland, “Waste Heat Recovery of Heavy-Duty Diesel Engines by Organic Rankine Cycle Part I: Hybrid Energy System of Diesel and Rankine Engines,” *SAE Int.*, vol. 1, no. 724, pp. 1–13, Apr. 2007.

[19] R. Freymann, “The Turbosteamer : A System Introducing the Principle of Cogeneration in Automotive Applications,” *MTZ*, vol. 69, no. 5, pp. 20–27, 2008.

[20] J. Galindo, S. Ruiz, V. Dolz, L. Royo-Pascual, R. Haller, B. Nicolas, and Y. Glavatskaya, “Experimental and thermodynamic analysis of a bottoming Organic Rankine Cycle (ORC) of gasoline engine using swash-plate expander,” *Energy Convers. Manag.*, vol. 103, pp. 519–532, Oct. 2015.

[21] J. Galindo, V. Dolz, L. Royo-Pascual, R. Haller, and J. Melis, “Modeling and experimental validation of a volumetric expander suitable for waste heat recovery from an automotive internal combustion engine using an organic Rankine cycle with ethanol,” *Energies*, vol. 9, no. 4, 2016.

[22] R. Lutz, P. Geskes, E. Pantow, and J. Eitel, “Use of Exhaust Gas Energy in Heavy trucks using the rankine process,” *MTZ*, vol. 73, pp. 32–37, 2012.

[23] F. Willems, F. Kupper, G. Rascanu, and E. Feru, “Integrated Energy and Emission Management for Diesel Engines with Waste Heat Recovery Using Dynamic Models,” *Oil Gas Sci. Technol. – Rev. d’IFP Energies Nouv.*, vol. 70, no. 1, pp. 143–158, Apr. 2014.

[24] H. Xie and C. Yang, “Dynamic behavior of Rankine cycle system for waste heat recovery of heavy duty diesel engines under driving cycle,” *Appl. Energy*, vol. 112, pp. 130–141, Dec. 2013.

[25] A. a. Boretti, “Transient operation of internal combustion engines with Rankine waste heat recovery systems,” *Appl. Therm. Eng.*, vol. 48, pp. 18–23, Dec. 2012.

[26] D. Wei, X. Lu, Z. Lu, and J. Gu, “Dynamic modeling and simulation of an Organic Rankine Cycle (ORC) system for waste heat recovery,” *Appl. Therm. Eng.*, vol. 28, pp. 1216–1224, 2008.

[27] T. A. Horst, W. Tegethoff, P. Eilts, and J. Koehler, “Prediction of dynamic Rankine Cycle waste heat recovery performance and fuel saving potential in passenger car applications considering interactions with vehicles’ energy management,” *Energy Convers. Manag.*, vol. 78, pp. 438–451, Feb. 2014.